

Recoverable creep deformation and transient local stress concentration due to heterogeneous grain-boundary diffusion and sliding in polycrystalline solids

Yujie Wei, Allan F. Bower^{*}, Huajian Gao^{**}

Division of Engineering, Brown University, Box D, Providence, RI 02912, USA

Received 8 June 2007; received in revised form 14 August 2007; accepted 15 August 2007

Abstract

Numerical simulations are used to investigate the influence of heterogeneity in grain-boundary diffusivity and sliding resistance on the creep response of a polycrystal. We model a polycrystal as a two-dimensional assembly of elastic grains, separated by sharp grain boundaries. The crystal deforms plastically by stress driven mass transport along the grain boundaries, together with grain-boundary sliding. Heterogeneity is idealized by assigning each grain boundary one of two possible values of diffusivity and sliding viscosity. We compute steady state and transient creep rates as functions of the diffusivity mismatch and relative fractions of grain boundaries with fast and slow diffusion. In addition, our results show that under transient conditions, flux divergences develop at the intersection between grain boundaries with fast and slow diffusivity, which generate high local stress concentrations. The stress concentrations develop at a rate determined by the fast diffusion coefficient, and subsequently relax at a rate determined by the slow diffusion coefficient. The influence of the mismatch in diffusion coefficient, loading conditions, and material properties on the magnitude of this stress concentration is investigated in detail using a simple model problem with a planar grain boundary. The strain energy associated with these stress concentrations also makes a small fraction of the plastic strain due to diffusion and sliding recoverable on unloading. We discuss the implications of these results for conventional polycrystalline solids at high temperatures and for nanostructured materials where grain-boundary diffusion becomes one of the primary inelastic deformation mechanisms even at room temperature.

© 2007 Published by Elsevier Ltd.

Keywords: Recoverable creep deformation; Grain-boundary diffusion; Grain-boundary sliding; Transient stress concentration

1. Introduction

Grain-boundary (GB) diffusion and sliding are the dominant mechanisms of plastic deformation in polycrystalline metals and ceramics at high homologous temperatures. They also contribute to room-temperature plastic flow in nanocrystalline materials, where the fine grain size tends to suppress plastic flow by

^{*}Corresponding author.

^{**}Also corresponding author.

E-mail addresses: allan_bower@brown.edu (A.F. Bower), huajian_gao@brown.edu (H. Gao).

dislocation motion while the high density of GBs accelerates diffusional creep. In addition, GB diffusion plays an important role in stress generation and relaxation in polycrystalline thin films.

GB diffusional creep in macroscopic polycrystals has been extensively studied. Nabarro (1948) and Herring (1950) first pointed out that self-diffusion can cause crystals to change shapes and induce macroscopic plastic deformation at elevated temperatures. Coble (1963) studied the dependence of macroscopic strain rates $\dot{\epsilon}$ on grain size l and applied tensile stress σ due to collective GB diffusion and showed that

$$\dot{\epsilon} = \alpha \frac{\delta D \Omega \sigma}{k_B T l^3}, \quad (1)$$

where α is a geometrical constant, D is the GB diffusivity and δ is the thickness of a layer in which interface diffusion is supposed to take place; k_B , T and Ω are the Boltzmann constant, the absolute temperature and the atomic volume, respectively. Ashby and Verrall (1973) considered a geometrical model of creep flow taking into account strains due to GB diffusion and sliding, to reflect the fact that both GB diffusion and sliding plays an increasingly important role in the inelastic deformation of polycrystalline solids as the temperature rises or the grain size decreases. More recent work has extended the original Coble model by accounting for phenomena such as interface reactions (Ashby, 1969, 1972; Arzt et al., 1983; Cocks, 1992). In general, these models predict a nonlinear relationship between stress and strain rate.

Numerical methods have been developed to study GB diffusion and associated mechanical behavior in polycrystalline solids. Needleman and Rice (1980) have first applied the finite-element method in modeling GB diffusion and creep. Pan and Cocks (1993) developed finite-element formulations for modeling GB diffusion in arbitrary networks of grains with straight GBs. They applied the numerical techniques, combined with a time integration algorithm, to study microstructure evolution during superplastic deformation in polycrystalline materials. Bower and Wininger (2004) extended the work of Pan and Cocks (1993) by using an advancing front algorithm to generate a sequence of adaptive, evolving finite-element meshes to solve the evolution of two-dimensional geometries. Sethian and Wilkening (2003) and Wilkening et al. (2004a,b) have used techniques from semigroup theory to study mass transport in microelectronic circuits due to electromigration and GB diffusion.

GB diffusion is also an important stress relaxation mechanism in thin films based on experimental observations (Thouless et al., 1996; Kobrinsky and Thompson, 1998) and theories (Gao et al., 1999; Weiss et al., 2001; Guduru et al., 2003). Meanwhile, it has been observed to act in combination with other deformation mechanisms in thin films. For example, recent studies on the mechanical behaviors of polycrystalline thin films on substrates (Gao et al., 1999) have indicated that constrained GB diffusion¹ induces crack-like singular stress fields which leads to novel dislocation mechanisms that are driven by locally induced, rather than globally applied, stresses. In situ TEM experiments (Balk et al., 2003), atomistic simulations (Buehler et al., 2003) and discrete dislocation simulations (Hartmaier et al., 2005) have shown that such constrained GB diffusion and the associated dislocation mechanisms dominate plastic deformation mechanisms in unpassivated films thinner than a few hundred nanometers. These studies are calling for broader investigations on the general importance of constrained GB diffusion mechanisms in polycrystalline materials. Coble-type GB diffusional creep, together with GB sliding accommodated by GB diffusion, have been considered as major deformation mechanisms in nanocrystalline materials by many authors (e.g., Gleiter, 1989). Although diffusion-controlled processes are typically activated only at high homologous temperatures, Yamakov et al. (2002) have argued, based on their molecular dynamics simulations, that Coble-creep should be a dominating mechanism in nanocrystalline materials even at low homologous temperatures. An important feature of plastic deformation controlled by GB diffusion is that it gives rise to a strain-rate sensitivity on the order of 1. Although strain-rate sensitivity around 1 is rarely observed in regular tensile and compressive tests for nanocrystalline materials, significantly enhanced strain-rate sensitivity has been reported in both h.c.p. and f.c.c. nc materials. Nc Cu synthesized by Jiang et al. (2006) showed a rate sensitivity about $m = 0.104$ at room

¹In columnar grain structures in thin films on substrates, diffusion tends to generate stress singularities at the ends of GBs that terminate perpendicular to the substrate, if diffusion between thin films and substrates are constrained. These stress singularities may lead to dislocation emission and initiate delamination. GB diffusion in such a situation is termed as ‘constrained GB diffusion’.

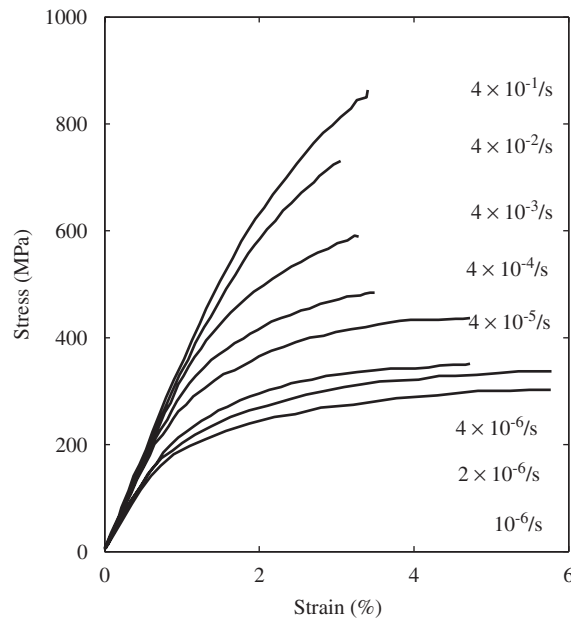


Fig. 1. Stress–strain curves of brush-plated nanocrystalline Cu at different strain rates. Data replotted from Jiang et al. (2006).

temperature in the strain rate range of $10^{-6}/s$ to $4 \times 10^{-1}/s$, Fig. 1. The authors have attributed the high strain-rate sensitivity to the dominant unstructured high-angle GBs in the material.

With the current technological trends in continuing miniaturization of structures in electronic devices and materials, a thorough understanding of the inelastic deformation mechanisms by GB diffusion and GB sliding is becoming increasingly important. On the other hand, existing experiments and theories have not been able to fully capture the complex interplay between different deformation mechanisms in GBs. In particular, the following issues are of interest for the present study.

- Most existing theories have assumed homogeneous diffusivity in GBs. In reality, most material properties are heterogeneous at the scale of individual grains; high angle, relatively unstructured GBs usually have higher diffusivities compared to low angle, structured GBs. GB diffusivity in a polycrystalline solid could differ by several orders of magnitude from one grain to another. Constrained GB diffusion due to heterogeneous diffusivities can affect not only deformation mechanisms in GBs, but also those in grain interiors.
- Diffusional deformation in GBs is a *kinetic process* but existing theories are usually developed for steady-state creep which neglects transient effects in GB diffusion. On the other hand, a number of important phenomena, such as stress concentration at GB junctions, could occur in a transient time period and disappear at steady state. In such cases, further progress will be required for more rigorous modeling of stresses induced by heterogeneous GB diffusion.
- GB sliding accommodated by diffusion is not considered in most theoretical models; GBs are either assumed to slide freely or not allowed to slide at all. These two extreme cases cannot represent real deformation behaviors in GBs.
- Constitutive laws for creep in polycrystalline solids have been based on simple boundary-value problems. In the presence of heterogeneous diffusive behaviors at the scale of individual grains, there is strong coupling of localized deformation mechanisms which cannot be predicted by a macroscopic analysis. An example is the constrained GB diffusion and the associated dislocation mechanisms in thin films (Gao et al., 1999; Balk et al., 2003; Buehler et al., 2003; Hartmaier et al., 2005).

Motivated by these issues, the objective of the present study is to address the mechanical behavior associated with heterogeneous GB diffusion and diffusion accommodated GB sliding. The plan of the paper is as follows. The computational method of investigation will be discussed in Section 2 and used to investigate deformation

behaviors induced by heterogeneous GB diffusion in Section 3. A generalized Maxwell model is adopted to interpret the numerical results in Section 4. Section 5 closes the paper with some concluding remarks.

2. Problem formulation and numerical method of investigation

We model a polycrystal as a two-dimensional assembly of elastic grains, separated by sharp GBs. The polycrystal is subjected to plane strain deformation with infinitesimal strains. Deformation in grains is modeled with anisotropic elasticity and dislocation mechanisms are suppressed. The crystal deforms plastically by stress driven mass transport along the GBs, together with GB sliding. Heterogeneity is idealized by assigning each GB one of two possible values of diffusivity and sliding viscosity. We compute steady state and transient creep rates as functions of the diffusivity mismatch and relative fractions of GBs with fast and slow diffusion. In the following, we briefly discuss the numerical method to investigate constrained GB diffusion. The reader is referred to Bower and Wininger (2004) for a detailed description of a more general formulation for modeling migration, diffusion, sliding of GBs as well as plastic deformation in grain interiors. The discussions below will focus on GB diffusion and GB sliding.

2.1. GB diffusion

For the GB shown in Fig. 2, the chemical potential per atom can be expressed as a function of time t and position s along the GB as (Herring, 1950)

$$\mu(s, t) = \mu_0 - \sigma_n(s, t)\Omega, \tag{2}$$

where $\sigma_n(s, t)$ denotes the normal traction at s , and μ_0 is a reference potential which can be taken as zero for the present study. Contributions from strain energy terms to the chemical potential are ignored in the above equation because they are small. The Nernst–Einstein equation for atomic flux $j(s, t)$ at s is

$$j(s, t) = -\frac{\delta D}{k_B T \Omega} \frac{\partial \mu(s, t)}{\partial s} = \frac{\delta D}{k_B T} \frac{\partial \sigma_n(s, t)}{\partial s} \tag{3}$$

and $\Omega j(s, t)$ gives the volumetric rate of diffusion in the GB for $j(s, t)$ denoting number of atoms crossing unit length of the GB. Mass conservation requires that the rate of material accumulation at s is related to the divergence of volumetric flux as

$$\frac{\partial u_n}{\partial t} = -\frac{\partial \Omega j(s, t)}{\partial s}, \tag{4}$$

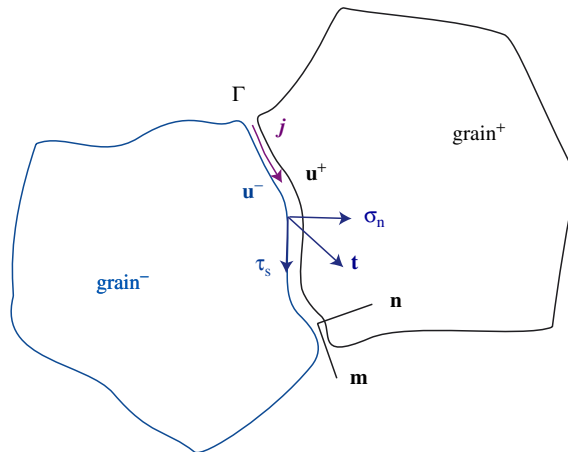


Fig. 2. A GB Γ with displacement \mathbf{u}^- and \mathbf{u}^+ at two sides, atomic flux is denoted by j . Here (\mathbf{m}, \mathbf{n}) defines a local coordinate with $\mathbf{n} = (n_1, n_2)$ along the GB normal and $\mathbf{m} = (m_1, m_2)$ along the tangential direction, and \mathbf{t} denotes the traction exerted on the surface belonging to grain⁻. It has a normal part σ_n and a shear component τ_s , i.e., $\mathbf{t} = \sigma_n \mathbf{n} + \tau_s \mathbf{m}$.

where $u_n = (\mathbf{u}^+ - \mathbf{u}^-) \cdot \mathbf{n}$ is the width of new material being inserted at point s due to diffusion. Combining with Eq. (3), the above equation could be rewritten as

$$\frac{\partial u_n}{\partial t} = -\frac{\delta D \Omega}{k_B T} \frac{\partial^2 \sigma_n(s, t)}{\partial s^2}. \quad (5)$$

Using $\tilde{u}_n = u_n/l$, $\tilde{s} = s/l$, $\tilde{t} = t/t_0$, $\tilde{\sigma} = \sigma/E^*$, Eq. (5) can be normalized as

$$\frac{\partial \tilde{u}_n}{\partial \tilde{t}} = -\tilde{D} \frac{\partial^2 \tilde{\sigma}_n(\tilde{s}, \tilde{t})}{\partial \tilde{s}^2} \quad \text{with} \quad \tilde{D} \equiv \frac{D}{D_0}, \quad (6)$$

where l is the averaged grain size, and $t_0 = k_B T l^3 / \delta D_0 \Omega E^*$ is a characteristic time controlling diffusional process in a GB with diffusivity of D_0 , and $E^* = E/(1 - \nu^2)$ is the plane strain modulus. In contrast to D , which represents the diffusivity of any GB in a heterogeneous system, D_0 is usually taken as a characteristic GB diffusivity in the system. Real physical data for D_0 , E , and ν used in this paper are listed in Table 1.

2.2. GB sliding

There are two types of GB sliding. One of them is a thermally activated, rate-dependent process; the other may be referred as athermal GB sliding, which is a temperature independent process involving relative sliding of two GBs when the resolved shear stress overcomes a threshold resistance. The athermal GB sliding differs from thermally activated sliding in that it is essentially rate-independent. In our analysis, only thermally assisted GB sliding is taken into consideration. A Newtonian viscous type of GB sliding is assumed with

$$\eta \frac{\partial u_s}{\partial t} = \tau_s. \quad (7)$$

The dimensionless expression of Eq. (7), with $\tilde{u}_s = u_s/l$, $\tilde{t} = t/t_0$ and $\tilde{\tau}_s = \tau/E^*$, is given as

$$\frac{\partial \tilde{u}_s}{\partial \tilde{t}} = \tilde{\eta} \tilde{\tau}_s \quad \text{with} \quad \tilde{\eta} \equiv \frac{k_B T l^2}{\delta D_0 \Omega \eta}. \quad (8)$$

Table 1
Material parameters used for grain-boundary diffusion, grain-boundary sliding and grain interior deformation

Parameters for GB diffusion in Eq. (5)		Frost and Ashby (1982)
N_A	Avogadro constant	6.022×10^{23} /mol
k_B	Boltzman constant	1.38×10^{-23} J/K
T	Absolute temperature	500 K
Ω	Atomic volume of Cu	1.18×10^{-29} m ³
δ	Effective GB thickness involving diffusion	$\sim 10^{-9}$ m
D_c	Pre-coefficient of GB diffusivity	5.0×10^{-6} m ² /s
Q_v	Activation energy for GB diffusion	1.04×10^3 J/mol
l	Grain size	100 nm
D_0	GB diffusivity of Cu	$D_c \exp\left(-\frac{Q_v}{N_A k_B T}\right)$
Parameters for GB sliding in Eq. (7)		
η	Viscosity to GB sliding	
Elastic constants for Cu (isotropic)		
E	Young's modulus	135 GPa
ν	Poisson's ratio	0.30
Elastic-plastic constants for Cu (anisotropic)		Simmons and Wang (1971)
C_{11}	Elastic constant	170 GPa
C_{12}		124 GPa
C_{44}		75 GPa

The dimensionless coefficient $\tilde{\eta}$ corresponds a normalized inverse viscosity and will be referred to as the normalized GB fluidity. For calculations in this paper, we will assign one or two possible values of GB diffusivity D and sliding viscosity η to GBs to study mechanical behaviors induced by heterogeneous GB properties.

2.3. Diffusion in GB junctions

In a microstructure composed of multiple grains, a junction of three or more grains is usually a site of high stress concentration due to severely mismatched elastic properties of adjacent grains, in which cavitation or damage could be initiated. In the scope of this paper, no damage or GB decohesion will be considered. GB junctions serve as bridges for atoms to transfer between interconnected boundaries. Mass conservation in the junction requires that the sum of fluxes from all GBs meeting at the junction be zero. A strong constraint is applied in our numerical implementation to satisfy mass conservation and chemical potential continuity in any junction.

2.4. Finite-element implementation

For a body V with internal boundaries Γ , displacement discontinuities crossing boundaries may exist, as seen in Fig. 2. Let \mathbf{t} be the traction along a GB and $(\mathbf{v}^+ - \mathbf{v}^-)$ be the relative velocity between two sides of the GB (Fig. 2), the variation of generalized internal virtual power $\delta\mathcal{P}$ for the body is given as ²

$$\delta\mathcal{P} = \int_V \boldsymbol{\sigma} : \delta\dot{\boldsymbol{\varepsilon}} dV + \int_{\Gamma} \mathbf{t} \cdot (\delta\mathbf{v}^+ - \delta\mathbf{v}^-) ds, \tag{9}$$

where $\delta\mathbf{v}$ is a kinematically admissible virtual velocity field, $(\delta\mathbf{v}^+ - \delta\mathbf{v}^-)$ is the jump in virtual velocity across the GB, and $\delta\dot{\boldsymbol{\varepsilon}}$ is a virtual strain rate

$$\delta\dot{\boldsymbol{\varepsilon}} = \frac{1}{2}([\nabla\delta\mathbf{v}] + [\nabla\delta\mathbf{v}]^T). \tag{10}$$

To enforce displacement jumps due to GB diffusion in Eq. (6) and GB sliding in Eq. (8), we augment the virtual internal power principle with Lagrange multipliers $\delta\sigma_n$ and $\delta\tau_s$ (Bower and Wininger, 2004), corresponding to variations in normal and shear stress along Γ . They must be continuous along GBs but may have discontinuities across junctions. The internal virtual power can be rewritten as

$$\begin{aligned} \delta\mathcal{P} = & \int_V \boldsymbol{\sigma} : \delta\dot{\boldsymbol{\varepsilon}} dV + \int_{\Gamma} \mathbf{t} \cdot (\delta\mathbf{v}^+ - \delta\mathbf{v}^-) ds \\ & + \int_{\Gamma} \left(\frac{\Delta u_n}{\Delta t} + D \frac{\partial^2 \sigma_n}{\partial s^2} \right) \delta\sigma_n ds + \int_{\Gamma} \left(\frac{\Delta u_s}{\Delta t} - \eta\tau_s \right) \delta\tau_s ds, \end{aligned} \tag{11}$$

where the Δ prefix of a variable indicates its change from one time step to the next. We separate the variation of virtual internal power in Eq. (11) into two parts

$$\delta\mathcal{P} = \delta\mathcal{P}_v + \delta\mathcal{P}_{gb} \tag{12}$$

with

$$\delta\mathcal{P}_v = \int_V \boldsymbol{\sigma} : \delta\dot{\boldsymbol{\varepsilon}} dV \tag{13}$$

representing the contribution by continuum elements in grain interiors and

$$\delta\mathcal{P}_{gb} = \int_{\Gamma} \mathbf{t} \cdot (\delta\mathbf{v}^+ - \delta\mathbf{v}^-) ds + \int_{\Gamma} \left(\frac{\Delta u_n}{\Delta t} + D \frac{\partial^2 \sigma_n}{\partial s^2} \right) \delta\sigma_n ds + \int_{\Gamma} \left(\frac{\Delta u_s}{\Delta t} - \eta\tau_s \right) \delta\tau_s ds \tag{14}$$

²Here equations are written in dimensionless format. The ‘~’ used in Eqs. (6) and (8) indicating dimensionless parameters is removed for convenience.

being the variation of virtual internal power contributed by boundaries. Integrating Eq. (14) by parts and using Eq. (3), we obtain

$$\begin{aligned} \delta \mathcal{P}_{\text{gb}} = & \underbrace{\int_{\Gamma} \mathbf{t} \cdot (\delta \mathbf{v}^+ - \delta \mathbf{v}^-) ds + \int_{\Gamma} \frac{\Delta u_n}{\Delta t} \delta \sigma_n ds - \int_{\Gamma} D \frac{\partial \sigma_n}{\partial s} \frac{\partial \delta \sigma_n}{\partial s} ds + \int_{\Gamma} \left(\frac{\Delta u_s}{\Delta t} - \eta \tau_s \right) \delta \tau_s ds}_{\text{by GB elements}} \\ & + \underbrace{\sum_{\alpha \in \partial \Gamma} j_{\alpha} \delta \sigma_n}_{\text{by junction elements}} \end{aligned} \quad (15)$$

Hence the variation of virtual internal power can be further divided into three parts

$$\delta \mathcal{P} = \delta \mathcal{P}_v + \delta \mathcal{P}_{\Gamma} + \delta \mathcal{P}_J, \quad (16)$$

where

$$\delta \mathcal{P}_{\Gamma} = \int_{\Gamma} \mathbf{t} \cdot (\delta \mathbf{v}^+ - \delta \mathbf{v}^-) ds + \int_{\Gamma} \frac{\Delta u_n}{\Delta t} \delta \sigma_n ds - \int_{\Gamma} D \frac{\partial \sigma_n}{\partial s} \frac{\partial \delta \sigma_n}{\partial s} ds + \int_{\Gamma} \left(\frac{\Delta u_s}{\Delta t} - \eta \tau_s \right) \delta \tau_s ds, \quad (17)$$

$$\delta \mathcal{P}_J = \sum_{\alpha \in \partial \Gamma_1} j_{\alpha} \delta \sigma_n + \sum_{\alpha \in \partial \Gamma_0} j_{\alpha} \delta \sigma_n \quad (18)$$

correspond to the contribution from continuum elements in grain interiors, GB elements, and elements in boundary junctions, respectively. Here $\partial \Gamma$ denotes all ends of GBs, which includes both junctions in the body ($\partial \Gamma_1$) and those in a sample's surfaces ($\partial \Gamma_0$). Unless stated otherwise, a symmetry boundary condition will be applied for GB junctions of the latter case, i.e., $j_{\alpha} = 0$ in $\partial \Gamma_0$. The normal stress σ_n must be equal at the ends of the three GBs that meet at a triple junction for chemical potential continuity. This condition is enforced using a constraint.

The coupled grain interior and GB deformation problem satisfies the following variational principle:

$$\delta \mathcal{P} = 0 \quad (19)$$

to first order in $\delta \mathbf{v}$, $\{\delta \sigma_n, \delta \tau_s\}$. Using the Galerkin method, the variations of internal power components, $\delta \mathcal{P}_{\Gamma}$ and $\delta \mathcal{P}_J$, can give the stiffness and residual for GB elements and junction elements, respectively. We have implemented the above numerical procedure in the commercial finite-element computer program ABAQUS/Standard (Abaqus Reference Manuals, 2005) via user element subroutines. In the next section, we will apply the constitutive models and numerical scheme introduced above to study the effects of heterogeneity in GB diffusivity and sliding resistance on the creep response of a polycrystal.

3. Heterogeneous GB diffusion and GB sliding

In a polycrystal with plastic deformation exclusively accommodated by GB diffusion and sliding, these two processes occur concurrently. The macroscopic mechanical behavior of the solid is governed by the cooperation and competition between diffusion and sliding in individual GBs. To define a local measure of relative importance of diffusion versus sliding in a GB, we consider the ratio R between normalized GB diffusivity (Eq. (6)) and GB fluidity (Eq. (8)), i.e.,

$$R = \frac{\tilde{D}}{\tilde{\eta}} = \frac{\delta D \Omega \eta}{k_B T l^2}. \quad (20)$$

In a GB with $R = 1$, for example, the local deformation rates by diffusion and sliding are comparable; while if $R = 0.01$, the local deformation rate by GB diffusion is about two orders of magnitude slower than that by GB sliding. Macroscopically, GB sliding is expected to be the rate controlling mechanism if $R \gg 1$ (corresponding to fast diffusion or high viscosity to GB sliding), and GB diffusion is the rate-controlling mechanism when $R \ll 1$. Note that the GB sliding velocity is directly proportional to the local shear traction

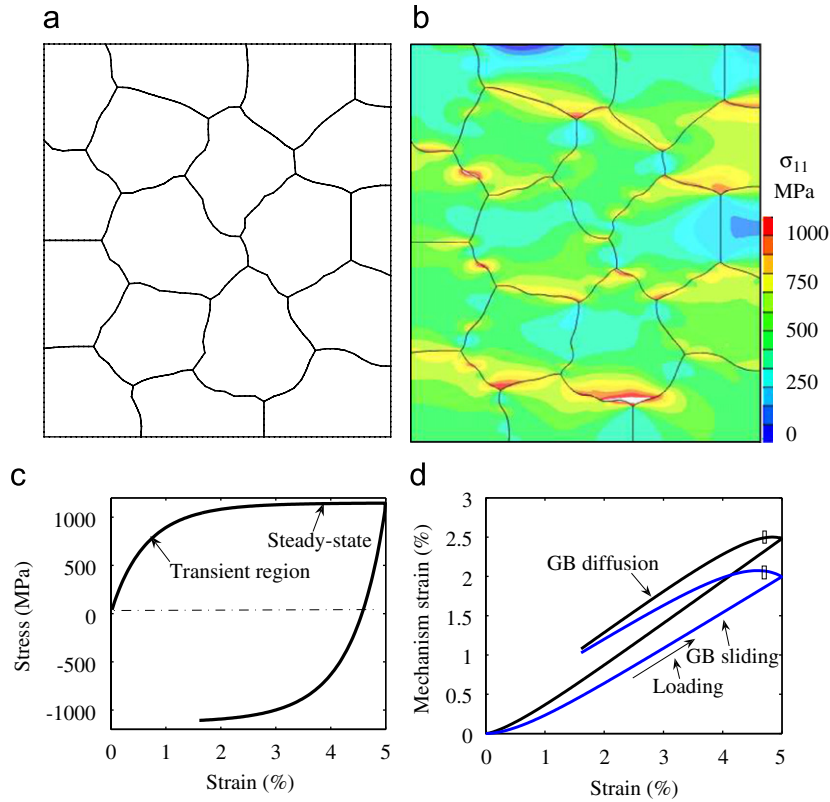


Fig. 3. Representative deformation behavior in polycrystalline solids with GB diffusion and sliding: (a) the microstructure; (b) stress contour (σ_{11}) at a total tensile strain of 1% showing stress concentration at triple junctions during the transient period; (c) the stress–strain curve showing a transient response followed by steady-state creep; (d) the evolution of mechanism strains by GB diffusion ($\epsilon_{11}^{\text{gbd}}$) and GB sliding ($\epsilon_{11}^{\text{gbs}}$) during a loading cycle. The square markers indicate points of zero macroscopic stress.

(Eq. (8)) while diffusional creep is controlled by the gradient in local normal stress (Eq. (6)), with different characteristic relaxation times for each process.

In order to illustrate the essential features of the mechanical behavior of a polycrystal deforming plastically by GB diffusion and sliding, we present first a representative simulation for a model of polycrystalline Cu with *homogeneous* GBs. In these simulations, uniform GB diffusion is assumed, i.e., $D/D_0 = 1$, D_0 being the GB diffusivity for polycrystalline Cu at $T = 500$ K. The viscosity of GB sliding is chosen to satisfy $R = 1$. As a specific example, we simulate GB diffusion and sliding controlled plastic deformation in polycrystalline Cu with an averaged grain size³ of $l = 100$ nm and at temperature $T = 500$ K. The parameters used are listed in Table 1. The microstructure used is shown in Fig. 3a. Nodes along the left boundary are fixed in the horizontal direction and those along the bottom are fixed in the vertical direction. A 5% tensile strain is applied to the sample in the horizontal direction at a strain rate of $10^{-4}/\text{s}$, followed by an unloading and subsequent compression at a strain rate of $-10^{-4}/\text{s}$. Contours of the stress component σ_{11} at a tensile strain of 1% during the transient stage is shown in Fig. 3b. Note the high stress concentrations near triple junctions. The macroscopic stress–strain curve (computed from the relative displacement of the boundaries of the specimen, and the resultant forces applied to the boundaries) is given in Fig. 3c, which shows a transient period followed by steady-state creep. Our computations also allow us to calculate the contribution to the total plastic strain arising from the various processes that contribute to the deformation (we shall subsequently refer to these as ‘mechanism strains’). The plastic strain rates due to GB sliding and

³The size of the i th grain is estimated by equating the area of the grain to $\pi l_i^2/4$. The averaged grain size l of a sample is the numerical average of l_i over all grains.

diffusion can be computed from

$$\dot{\epsilon}_{ij}^{\text{gbd}} = \frac{1}{V} \int_{\Gamma} \frac{(\Delta \mathbf{u}^+ - \Delta \mathbf{u}^-) \cdot \mathbf{n}}{\Delta t} n_i n_j ds, \quad \epsilon_{ij}^{\text{gbd}} = \int_0^t \dot{\epsilon}_{ij}^{\text{gbd}} dt, \quad (21a)$$

$$\dot{\epsilon}_{ij}^{\text{gbs}} = \frac{1}{V} \int_{\Gamma} \frac{(\Delta \mathbf{u}^+ - \Delta \mathbf{u}^-) \cdot \mathbf{m}}{\Delta t} \frac{(n_i m_j + m_j n_i)}{2} ds, \quad \epsilon_{ij}^{\text{gbs}} = \int_0^t \dot{\epsilon}_{ij}^{\text{gbs}} dt, \quad (21b)$$

where V is the total volume of the sample and Γ is the network consisting of all GBs. Under steady-state conditions, the total strain rate is equal to the sum of these two quantities. Under transient conditions, there is an additional contribution to the strain rate from the elastic deformation within the grains. Fig. 3d gives the evolution of the strain rates along the loading direction ($\dot{\epsilon}_{11}^{\text{gbd}}$ and $\dot{\epsilon}_{11}^{\text{gbs}}$) due to GB diffusion and sliding.

The rectangular markers in Fig. 3d indicate a zero macroscopic stress at that point. In what follows, we will further investigate steady state and transient creep rates as functions of the diffusivity mismatch and relative fractions of GBs with fast and slow diffusion.

3.1. Coble creep

In this subsection, we investigate Coble creep in a homogeneous polycrystal, in which all GBs have the same diffusivity and sliding resistance. In particular, our goal is to study the role of the relative rates of sliding and diffusion on the macroscopic creep behavior of the solid. When GB diffusion is the rate controlling mechanism in the material, stress σ as a function of strain e can be expressed as a dimensionless function

$$\frac{\sigma \delta D \Omega}{k_B T l^3 \dot{\epsilon}} = f\left(\frac{\delta D \Omega E}{k_B T l^3 \dot{\epsilon}} e, R\right), \quad (22)$$

where $\dot{\epsilon}$ is the applied strain rate. For a fixed R , it is expected that f will be a constant $f = 1/\alpha$ at steady-state creep as predicted in Eq. (1). In the case that GB sliding is the rate controlling mechanism, a similar dimensionless equation could be written in the form of

$$\frac{\sigma}{\eta l \dot{\epsilon}} = g\left(\frac{G}{\eta l \dot{\epsilon}} e, R\right), \quad (23)$$

where G is the shear modulus. The microstructure shown in Fig. 4a is adopted to study the strain-rate dependence of stress in polycrystals whereby plasticity is exclusively accommodated by GB diffusion and GB sliding. A uniform diffusivity of $D = D_0$ is used and $R = 1$ is chosen. Fig. 4b gives the stress strain curves at

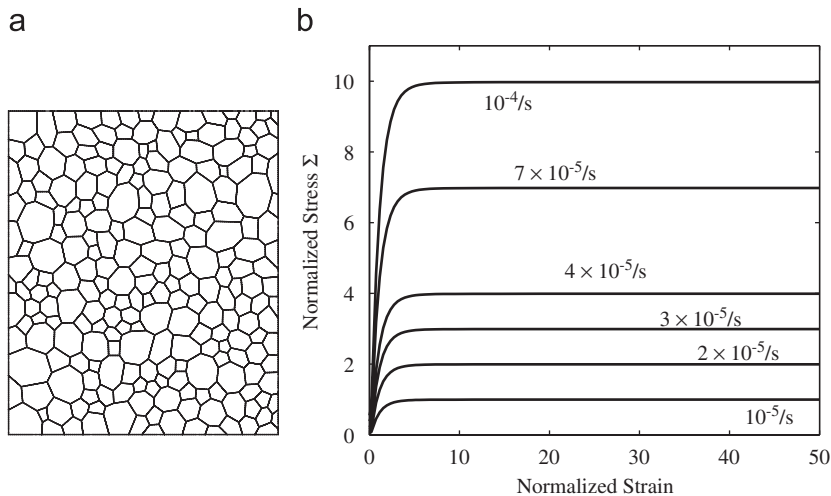


Fig. 4. Coble creep: (a) the adopted microstructure with 236 grains; (b) normalized stress–strain curves at different strain rates, $\Sigma = \sigma / (k_B T l^3 \dot{\epsilon} / \delta D \Omega)$ with $\dot{\epsilon} = 10^{-5}/s$. Strains for each curve are normalized by their respective characteristic strain $k_B T l^3 \dot{\epsilon} / \delta D \Omega E$.

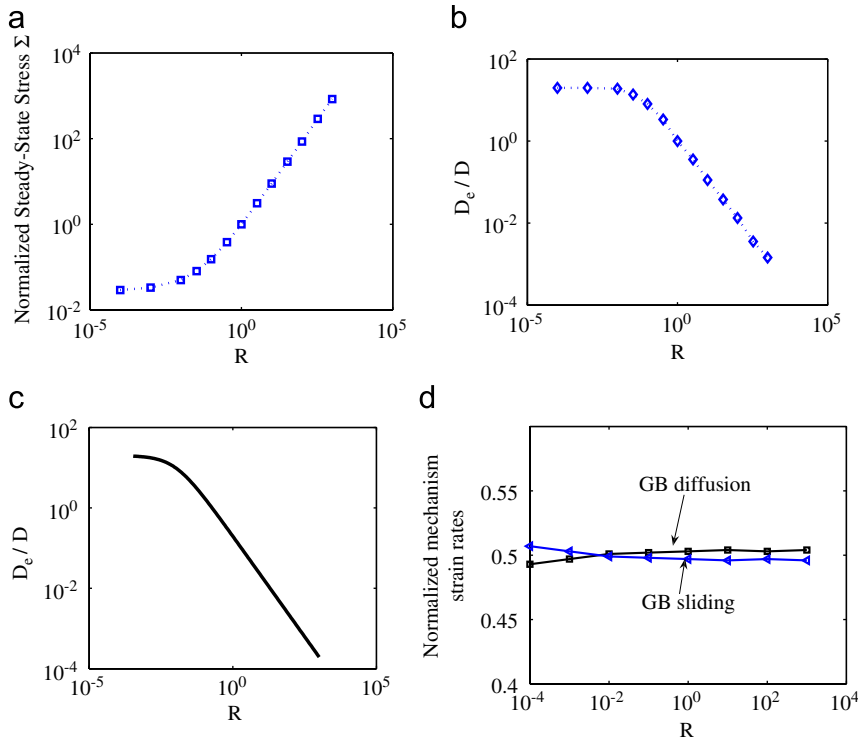


Fig. 5. Influence of the GB diffusivity–fluidity ratio R : (a) the steady-state stress Σ versus R , where $\Sigma = \sigma_{ss}/(k_B T l^3 \dot{\epsilon}/\delta D \Omega)$ and $\dot{\epsilon} = 10^{-5}/s$; (b) the “effective diffusivity” D_e versus R ; (c) the fitted curve for R and D_e using Eq. (26); (d) the mechanism strain rates at steady state versus R (mechanism strains are normalized by the applied strain rate $\dot{\epsilon} = 10^{-5}/s$).

different strain rates. Strain for each curve is normalized by $k_B T l^3 \dot{\epsilon}/\delta D \Omega E$, here $\dot{\epsilon}$ is the respective strain rate for each curve. Stresses in all curves have been normalized by $k_B T l^3 \dot{\epsilon}/\delta D \Omega$ with $\dot{\epsilon} = 10^{-5}/s$. The results show a clear dependence of stresses on strain rates, as in Eq. (1). Interestingly, the parameter α we obtained in the calculations is about 1, which is two orders of magnitude smaller than that given by Coble (1963) ($\alpha = 148$). There are two reasons for the discrepancy: first, Coble’s result is based on a three-dimensional analysis of spherical grains and second, the Coble result assumes free GB sliding. For a regular array of freely sliding two-dimensional hexagonal grains, $\alpha = 36$ (Spingarn and Nix, 1978). In simulations with vanishing GB viscosity ($R = 10^{-5}$) we obtain $\alpha = 34$ (Fig. 5b, $D_e/D \approx 34$ at $R = 10^{-5}$), which is close to the result for freely sliding grains.⁴ With $R = 1$, the viscosity of the GBs substantially reduces the rate of creep. The dependence of steady-state creep rate $\dot{\epsilon}$ on grain size l is self-evident by taking the right side of Eq. (22) to be a constant.

⁴It can be shown that the creep rate calculated with an average grain size of l is overestimated in a polycrystal with nonuniform grain size. To illustrate this with a simple model, consider N parallel dashpot elements, with the k th element representing the response of a grain with a given grain size l_k . Each element, based on Eq. (1), has a viscosity of $\eta_k = k_B T l_k^3 / \alpha \delta D \Omega$ where α is taken as a constant for a material of uniform grain size. Taking the macroscopic stress σ as an average over all elements ($\sigma = \sum \sigma_k / N$), we have

$$\dot{\epsilon} = \alpha \frac{\delta D \Omega \sigma}{k_B T ((1/N) \sum_{k=1}^N l_k^2)} < \alpha \frac{\delta D \Omega \sigma}{k_B T ((1/N) \sum_{k=1}^N l_k^3)}$$

which suggests that a polycrystal with a random distribution of grain sizes should creep more slowly than a perfect array of hexagonal grains. Here we have used the inequality (Hardy et al., 1934)

$$\left(\frac{1}{N} \sum_{k=1}^N l_k \right)^3 < \left(\frac{1}{N} \sum_{k=1}^N l_k^3 \right).$$

The collective plastic deformation by GB diffusion and sliding at grain level results in a macroscopic creep rate which can be written in the form of

$$\dot{\epsilon} = \frac{\delta D_e \Omega \sigma}{k_B T l^3}, \quad (24)$$

where D_e is a macroscopic “effective diffusivity” representing contributions from both diffusion and sliding at the grain level. Indeed, experimentally measured GB diffusivity is an “effective diffusivity” since diffusion and sliding may need to cooperate for compatible deformation, especially when dislocation activities are suppressed. We will justify this conclusion at the end of this subsection. We will find D_e in a polycrystal with specific GB properties through numerical experiments. Using a simple formula for elastic–viscoplastic solids that $\dot{\sigma} = E(\dot{\epsilon} - \dot{\epsilon})$, together with Eq. (24), we can derive the following stress–strain behavior for a polycrystal with GB diffusion and sliding being the exclusive plastic deformation mechanisms,

$$\frac{\sigma}{\sigma_{ss}} = 1 - \exp\left(-\frac{\delta D_e \Omega E}{k_B T l^3 \dot{\epsilon}} e\right), \quad (25)$$

where

$$\sigma_{ss} = k_B T l^3 \dot{\epsilon} / \delta D_e \Omega$$

denotes the corresponding steady-state stress as $t \rightarrow \infty$. Once a stress–strain curve in a polycrystal with specific material properties is obtained, we can extract σ_{ss} and D_e by fitting the stress–strain curve to Eq. (25). Indeed, a very good match is found between stress–strain curves from our numerical simulations and that described by Eq. (25) with appropriate σ_{ss} and D_e .

In the preceding calculations, we have assumed the GB diffusivity–fluidity ratio $R = 1$. Now we take R as a variable while fixing the GB diffusivity. We vary the viscosity associated with GB sliding to identify the rate controlling mechanism in the polycrystal at different R . With the stress–strain curve from our calculation for a given R , we can determine σ_{ss} and D_e by curve fitting using Eq. (25). Fig. 5a plots the relationship between steady-state stress (normalized by $k_B T l^3 \dot{\epsilon} / \delta D \Omega$ with $\dot{\epsilon} = 10^{-5}/s$) and R , while Fig. 5b plots that between D_e and R . Interestingly, Fig. 5b shows a negative slope of -1 indicating a linear relationship between D_e and $1/R$ for $R > 10^{-2}$, indicating that GB sliding remains to be the rate controlling mechanism even when GB fluidity is two orders of magnitude larger than GB diffusivity. In this region, the “effective diffusivity” could be related to the uniform GB diffusivity D by $D_e = D/R$. Further reducing GB sliding viscosity will shift the rate-controlling mechanism from GB sliding to GB diffusion. Our analysis suggests that the rate-controlling mechanism is GB sliding for $R > 10^{-2}$ and GB diffusion for $R < 10^{-2}$.

Despite the difference in R for the above calculations, the normalized mechanism strain rates shown in Fig. 5d indicate that GB diffusion and sliding play almost equally important roles in accommodating deformation at steady state.

A qualitative understanding of the roles of GB sliding and diffusion in controlling the macroscopic stress in the polycrystal can be obtained by representing the deformation mechanisms as two parallel spring–dashpot elements, to be discussed in more detail in Section 4. Under steady-state conditions the stress in the two elements is given by

$$\dot{\epsilon} = \begin{cases} A_d \sigma_{ed} & \text{diffusion element,} \\ A_s \sigma_{es} & \text{sliding element,} \end{cases}$$

where σ_{ed} and σ_{es} denote stresses in the diffusion and sliding element, respectively, and A_d and A_s are two coefficients that can be determined from the limiting cases of sliding and diffusion controlled deformation. Then the macroscopic response is

$$\dot{\epsilon} = \frac{2A_d A_s}{A_d + A_s} \sigma, \quad (26)$$

where $\sigma = (\sigma_{ed} + \sigma_{es})/2$ is the average macroscopic stress. The numerical results in Fig. 5b with R in the range of $(10^{-4}, 10^4)$ can be fit by Eq. (26) with $A_d = 10$, and $A_s = 0.1/R$, as shown in Fig. 5c. Eq. (26) is able to represent the trends in Fig. 5b reasonably well.

The investigations in this section indicate that creep in a polycrystal requires cooperative GB sliding and GB diffusion. Such a constraint may explain the limited ductility of polycrystalline materials where dislocation mechanisms are largely suppressed and plastic deformation is mainly accommodated by GB diffusion and sliding, e.g., ceramics and nanocrystalline materials.

3.2. Scaling behavior by heterogeneous GB diffusion and sliding

We next turn to investigate the influence of heterogeneous diffusivity on the macroscopic mechanical behavior. We will show that the saturation in stress–strain curves that commonly occurs in Coble creep changes character if there is no continuous fast diffusion path across the GB network. Heterogeneous GB diffusion in polycrystals is somewhat analogous to bond percolation. The flow of atoms in GBs can be compared to the flow of electricity through a network of resistors represented by GBs. Atoms (electricity) diffuse easily along paths of high diffusivity (low resistors) but may be blocked by low diffusivity GBs (high resistors). If there is no trans-system diffusive path in the sample, the Coble-type creep may not be achieved in the time scale of interest. We consider the microstructure shown in Fig. 6a. GBs with a square marker have a slow diffusivity of $10^{-10}D_0$ and the rest have D_0 . There is no cross-sample high diffusive path in this microstructure. The corresponding stress–strain curves at different strain rates, as shown in Fig. 6b, do not exhibit a Coble-type steady-state behavior.

Mechanical deformation in a polycrystal with heterogeneity in GB diffusion and sliding can be better understood by defining a dimensionless parametric function

$$\frac{\sigma \delta D_f \Omega}{k_B T l^3 \dot{\epsilon}} = f\left(\frac{\delta D_f \Omega E}{k_B T l^3 \dot{\epsilon}} e, R, \frac{D_f}{D_s}, \phi\right), \quad (27)$$

where D_f/D_s is the ratio of fast diffusivity over slow diffusivity and ϕ is the fraction of fast diffusion GBs. If we adopt Eq. (25) to describe overall stress–strain curves in the polycrystal, the “effective diffusivity” D_e may be represented by

$$D_e = g(D_s, D_f, \phi, R), \quad (28)$$

where g is an undetermined function. The relationship between σ and $\{D_s, D_f, \phi, R\}$ is condensed to its dependence on D_e . The microstructure in Fig. 4a is used to construct the dependence of D_e on these parameters in function g .

The influence of heterogeneity in GB diffusion and sliding on deformation in the microstructure has been investigated at three different cases: (a) Each GB is randomly assigned either a fast diffusivity D_f or a slow diffusivity D_s , with $D_f/D_0 = 1$ and $D_s/D_0 = 10^{-3}$. The viscosity of GB sliding is taken to make $R = 1$ in each

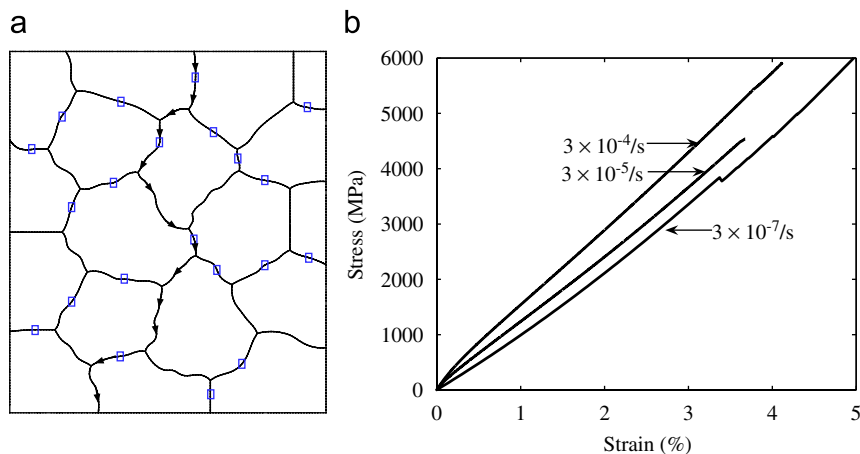


Fig. 6. Analogy between GB diffusion and percolation: (a) the adopted microstructure, GBs with a square marker may have a slow diffusion than others; (b) stress–strain curves at different loading rates.

boundary, in which case GB sliding is the rate-controlling mechanism. (b) The same GB diffusivity as in (a) except $R = 10^{-4}$ in each boundary. In this case, GB diffusion is the controlling mechanism. (c) The same arrangement with the fast diffusivity GBs as in (a) but the diffusion in slow diffusivity GBs is completely turned off. A loading rate of $\dot{\epsilon} = 10^{-5}/\text{s}$ is applied to all calculations.

Fig. 7 shows the stress–strain curves for different ϕ for case (a). The results show that higher stresses and larger strains are required to reach steady-state diffusion as ϕ decreases. (Similar behaviors exist for cases (b) and (c).) We then extracted the steady-state stress σ_{ss} and “effective diffusivity” D_e by fitting the calculated stress–strain curves to Eq. (25). Fig. 8a shows the steady-state stress versus ϕ for the three cases. When GB sliding is the rate controlling mechanism (case (a) with $R = 1$), there is no abrupt transition for steady-state stress as fast diffusion GB fraction ϕ increases. When GB diffusion is the rate-controlling mechanism, there is a region around $0.4 < \phi < 0.7$ with a quick transition from deformation controlled by fast diffusion GBs to that by slow diffusion GBs as ϕ increases, resembling a percolating system. In case (c), some GBs are completely constrained and the system shifts from GB accommodated creep to purely elastic deformation below a critical diffusive GB fraction. Fig. 8b plots the “effective diffusivity” D_e versus ϕ for the three cases.

The influence of D_f/D_s in Eq. (27) is also studied numerically. Fig. 9a shows the trends of steady-state stress versus D_f/D_s for several ϕ . Based on Eq. (25) and the known steady-state stress for each ϕ , Fig. 9b shows the relationship between “effective diffusivity” D_e and D_f/D_s for several ϕ .

3.3. Transient stress concentration by heterogeneous diffusivity and sliding

In this section, we focus on the influence of heterogeneous diffusivity on the microscopic stress field in the polycrystal. The main observation in this subsection is that, if the diffusivity changes abruptly at a point in the GB network, an applied load on the body induces transient crack-like stress concentrations at the time scale controlled by the fast diffusivity, which subsequently relax out of the system at a rate governed by the slow diffusivity. Similar behavior will be shown in the presence of heterogeneous GB sliding. We consider the simple idealized microstructure illustrated in Fig. 10: the polycrystal is approximated as an assembly of rectangular grains, with GBs oriented parallel and transverse to the loading direction. The GBs that are normal to the loading axis have a position-dependent diffusivity as indicated in the figure: the region between $-1 < x < 0$ has a fast diffusion coefficient D_f , while the region between $0 < x < 1$ has a slow diffusion coefficient D_s . $R = 1$ is maintained in the GB at any position. The vertical GBs are not modeled explicitly: instead, we assume that they act as perfect sources of flux, by enforcing the condition that the normal stress on the horizontal GB at $x = \pm 1$ equals zero. The solid may be subjected to either stress or strain loading in the vertical direction. Our main objective is to compute the variation of normal stress that acts on the horizontal GB.

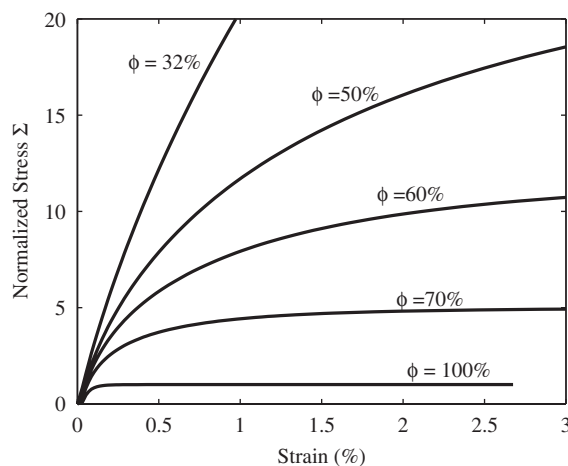


Fig. 7. Stress–strain curves for different fractions of fast diffusion GBs ϕ . Stresses are normalized as $\Sigma = \sigma / (k_B T^3 \dot{\epsilon} / \delta D_f \Omega)$ with $\dot{\epsilon} = 10^{-5}/\text{s}$. As ϕ decreases, higher stresses and larger strains are required to reach steady-state creep.

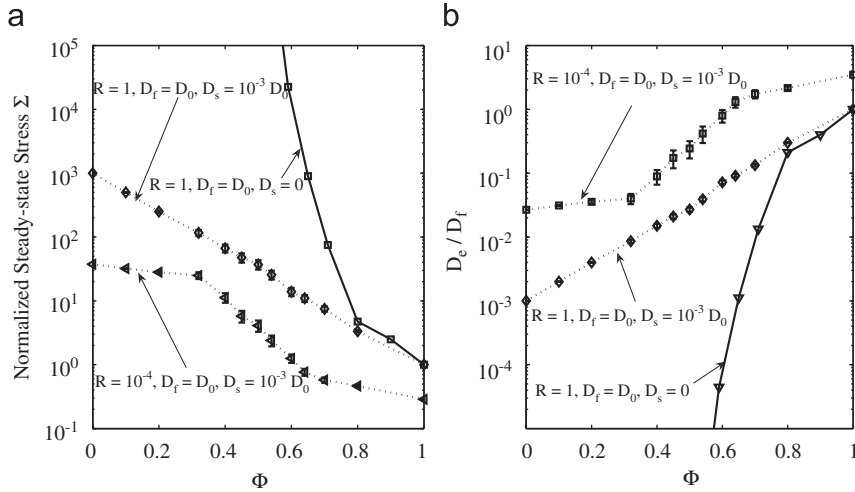


Fig. 8. GB diffusion in a bi-diffusivity polycrystal (error bars are based on three calculations at a given ϕ): (a) normalized steady-state stress ($\Sigma = \sigma_{ss}/(k_B T l^3 \dot{\epsilon}/\delta D_f \Omega)$ with $\dot{\epsilon} = 10^{-5}/s$) versus fast diffusivity GB fraction ϕ ; (b) “effective diffusivity” D_e versus ϕ .

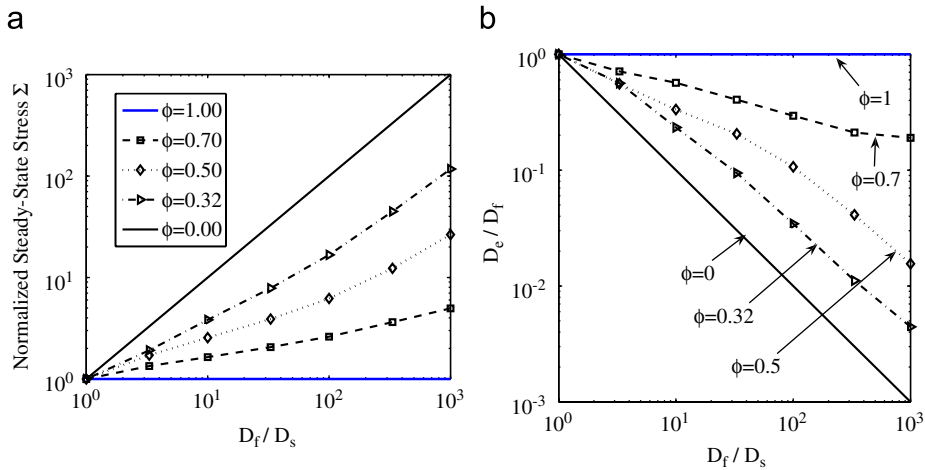


Fig. 9. Influence of D_f/D_s in a bi-diffusivity polycrystal: (a) normalized steady-state stress ($\Sigma = \sigma_{ss}/(k_B T l^3 \dot{\epsilon}/\delta D_f \Omega)$ with $\dot{\epsilon} = 10^{-5}/s$) versus D_f/D_s for several ϕ ; (b) “effective diffusivity” D_e versus D_f/D_s at several ϕ .

In particular, we shall show that the jump in diffusivity and viscosity at $x = 0$ generates a severe transient stress concentration.

The normal traction σ in the GB can be expressed in terms of a dimensionless function as

$$\frac{\sigma}{\sigma_\infty} = f\left(\frac{\delta D_f \Omega E}{k_B T l^3} t, \frac{D_f}{D_s}, \frac{\eta_h}{\eta_l}\right), \quad (29)$$

where σ_∞ is the applied stress and t is time.

To avoid introducing an extra time scale in the system using strain controlled loading, we use stress controlled loading to study the dependence of σ on time t in Eq. (29). We assign $D_f/D_s = 10^4$ and $D_f/D_0 = 20$ in the GB. A constant tensile stress of σ_∞ is applied to the sample at $t = 0$. The GB traction profiles at different snapshots are plotted in Fig. 11a. The history of normal traction in the GB shows four stages: (a) at $t = 0$ the stress is uniform; (b) a stress peak develops at very early times near $x = -1$ and propagates towards $x = 0$; (c) the stress drops to a very low value in the region $-1 < x < 0$, and simultaneously a stress concentration develops near $x = 0$ in the region $0 < x < 1$; (d) the stress concentration gradually attenuates as

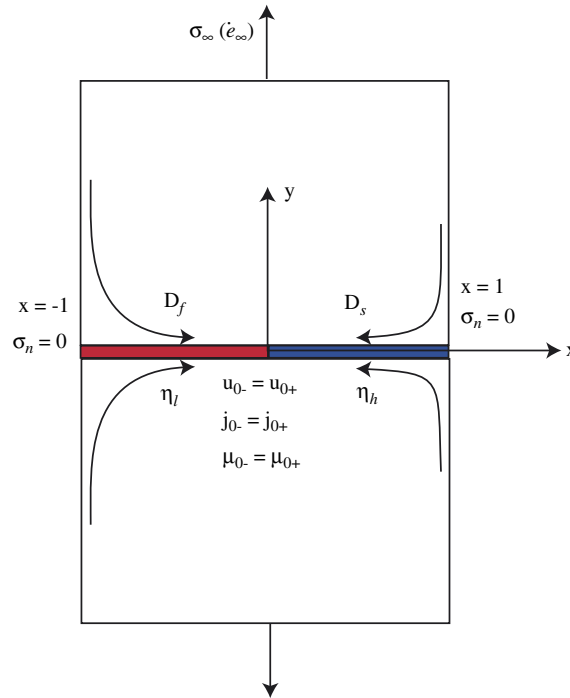


Fig. 10. A bi-diffusivity GB between two rectangular grains subjected to a constant strain rate $\dot{\epsilon}_\infty$ or stress σ_∞ in the far field. Diffusion along vertical GBs is assumed to be so rapid that $\sigma_n = 0$ along the two ends of the horizontal GB, which represent the limit of infinite vacancy sources/sinks. D_f and D_s are fast and slow diffusivities while η_h and η_l denote high and low viscosities. Displacement, flux and chemical potential at the junction are continuous.

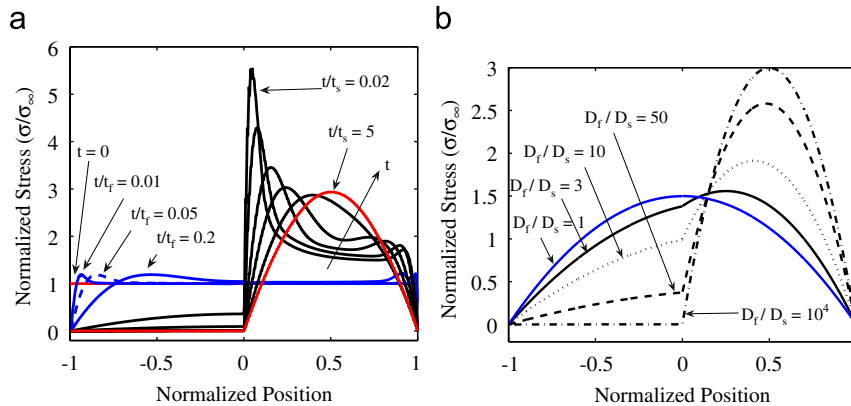


Fig. 11. Normal traction profiles in the GB at different times for the sample in Fig. 10 subjected to a constant tensile stress of $\sigma_\infty = 500$ MPa from $t = 0$: (a) transient stress concentration. The stress evolution has four characteristic periods, as detained in the text, $t_f = k_B T l^3 / E^* \delta D_f \Omega$ and $t_s = k_B T l^3 / E^* \delta D_s \Omega$; (b) Steady-state GB traction for several D_f and D_s .

the stress approaches the steady-state distribution. The two transients evolve with different characteristic time scales: the characteristic time for stress evolution in the region $-1 < x < 0$ is $t_f \approx k_B T l^3 / E^* \delta D_f \Omega$, while that in $0 < x < 1$ for relaxation to steady state is $t_s \approx k_B T l^3 / E^* \delta D_s \Omega$. Long term diffusion over the time scale of t_s is similar to that in classical steady-state creep models. The steady-state stress profile is well described by the analytical solution given in Eq. (31) in Appendix A. With $\sigma_\infty = 500$ MPa, Fig. 11b plots several steady-state normal traction profiles for different ratios of D_f/D_s based on Eq. (31).

Similar phenomena could be seen in the presence of heterogeneous GB sliding. We apply a constant shear stress τ_∞ at $t = 0$ to the top surface of the sample. In the low viscosity region, $\eta_l = k_B T l^2 / \delta D_0 \Omega$ and in the high viscosity region, $\eta_h = 10^3 \eta_l$. GB diffusivity in both regions is $D_f = D_s = D_0$. Fig. 12 plots shear traction profiles in the GB at different times, which resembles the normal traction profiles in the case of heterogeneous GB diffusion. The stress evolution shows three characteristic stages: (I) at very early times, relative high shear stress emerges over the entire boundary $-1 < x < 1$; (II) the stress drops to a very low value in the low viscosity region $-1 < x < 0$, and simultaneously an increasing stress concentration develops near $x = 0$ in the region $0 < x < 1$; (III) this stress concentration gradually attenuates as the stress approaches the steady-state distribution. The two transients evolve with different characteristic time scales: the characteristic time for stress evolution in the region $-1 < x < 0$ is $t_l \approx \eta_l l / G$, while that in $0 < x < 1$ for relaxation to steady state is $t_h \approx \eta_h l / G$.

The influence of the diffusivity ratio D_f/D_s on stress concentration is investigated by varying D_s while keeping D_f/D_0 fixed at unity. Since most experiments are conducted using strain controlled loading, we apply a constant strain rate of $\dot{\epsilon} = 10^{-4}/s$ to the sample shown in Fig. 10. Fig. 13a plots the normal traction along the GB in which $D_f/D_s = 100$. Severe stress concentration due to heterogeneous diffusion is observed in Fig. 13b when $D_f/D_s = 10^4$. Deformation in the low diffusivity GB cannot be accommodated by diffusion during the process, consequently giving rise to high stresses. As the difference in diffusivity in the two regions

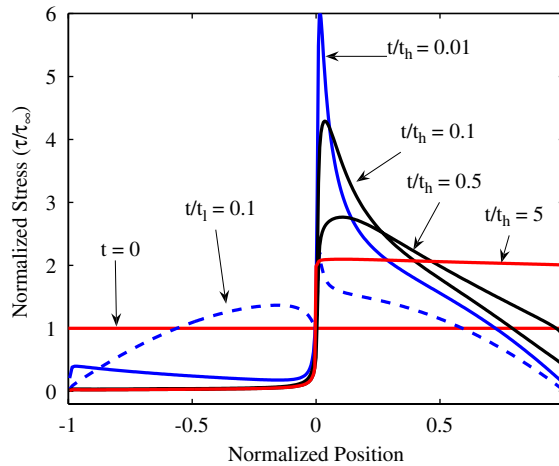


Fig. 12. Shear traction profiles in the GB at different times for the sample in Fig. 10 subjected to a constant shear of $\tau_\infty = 500$ MPa from $t = 0$. The stress evolution has three characteristic periods, as detailed in the text. Here $t_l \eta_l l / G$ and $t_h = \eta_h l / G$, hence $t_h = 10^3 t_l$ in this calculation.

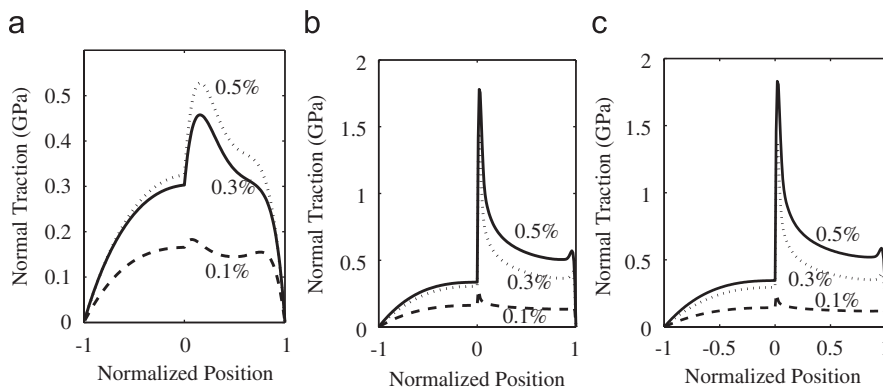


Fig. 13. Normal traction profiles at $\epsilon = 0.1\%$, 0.3% and 0.5% . The bi-diffusivity GB is loaded at a strain rate of $\dot{\epsilon} = 10^{-4}/s$. Diffusivity $D_f/D_0 = 1$ in the left half of the GB is fixed. (a) $D_f/D_s = 10^2$; (b) $D_f/D_s = 10^4$; (c) $D_f/D_s = 10^2$ but $\dot{\epsilon} = 10^{-2}/s$.

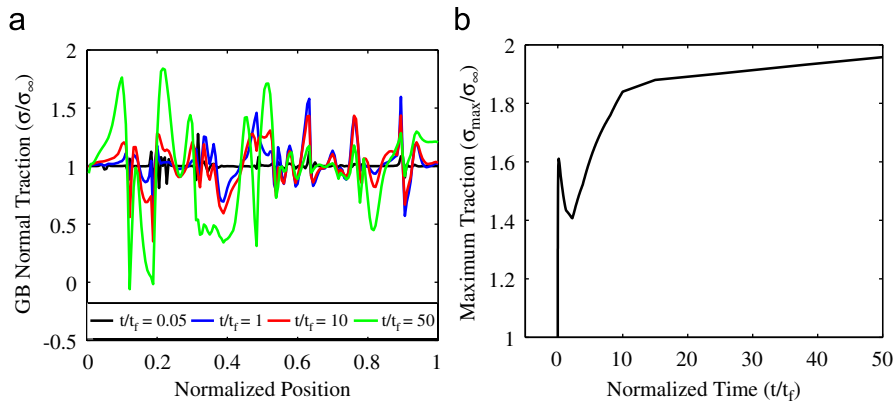


Fig. 14. Stress-fluctuation in a polycrystal with bi-diffusivity in GBs. (a) GB normal tractions (normalized by the applied stress $\sigma_\infty = 500$ MPa) along the trajectory shown in Fig. 6a at several snapshots. (b) The evolution of maximum GB normal traction in the polycrystal.

becomes larger, the high diffusivity GB essentially becomes a crack over the characteristic time associated with diffusion on this boundary, inducing high stress concentration in the low diffusivity GB. Larger D_f/D_s and/or η_h/η_l gives rise to higher σ .

Also, higher strain rates induce higher stress concentrations under the present assumption of no plastic deformation in the grain interiors, as indicated by Figs. 13a and c. These two calculations are performed with the same GB properties but at different loading rates.

We further simulated stress evolution in a polycrystal sample with heterogeneous GB diffusivity. The structure shown in Fig. 6a is adopted. GBs with square markers have diffusivity of D_s and the rest have D_f , with $D_f/D_s = 10^4$ and $D_f/D_0 = 20$. The diffusivity–fluidity ratio $R = 1$ is maintained for each GB. A constant tensile stress σ_∞ is exerted on the right side. Normalized GB normal traction along black arrows in Fig. 6b at several snapshots are shown in Fig. 14a. Small stress peaks develop in some fast diffusion GBs at very early stage ($t/t_f = 0.05$). These peaks dissipate quickly as loads are shifted to low diffusivity GBs. At the end, most loads are carried by the slow diffusion GBs. Note the high stress fluctuation along GBs. Fig. 14b plots the evolution of the maximum GB normal traction in the polycrystal. A peak at the early stage is observed in slow diffusion GBs. For such a large system, we have not taken the mesh size and time step sufficiently small to fully capture the transient stress concentration. In this sense, we expect a higher stress concentration if the mesh size and time step are taken to be smaller. The saturated peak stress indicates that the system is approaching steady-state creep in slow diffusion GBs. The transient stress concentration shown in the polycrystal is qualitatively consistent with the analysis for a single GB shown in Fig. 10.

The behaviors of transient stress concentration for deformation accommodated by heterogeneous GB diffusion and sliding provide an explanation why nanostructured materials tend to be more ductile at lower strain rates (Cheng et al., 2005; Wei and Anand, 2007). If GB diffusion and sliding are dominant plastic deformation mechanisms, materials deformed at lower strain rates have lower risks of crack initiation and growth in GBs. In contrast, high strain rates tend to induce severe stress concentrations at GB junctions and give rise to higher risks of GB fracture, rendering the materials more brittle.

3.4. Recoverable creep deformation by diffusion and sliding

In this section, we will show that inelastic deformation by heterogeneous GB diffusion and sliding in polycrystalline solids can be partially recoverable. As seen in Section 3.2, there may be severe stress concentration in a polycrystal with heterogeneous GB diffusion and sliding viscosity. The strain energy associated with these stress concentrations can make a fraction of the plastic strain due to diffusion and sliding

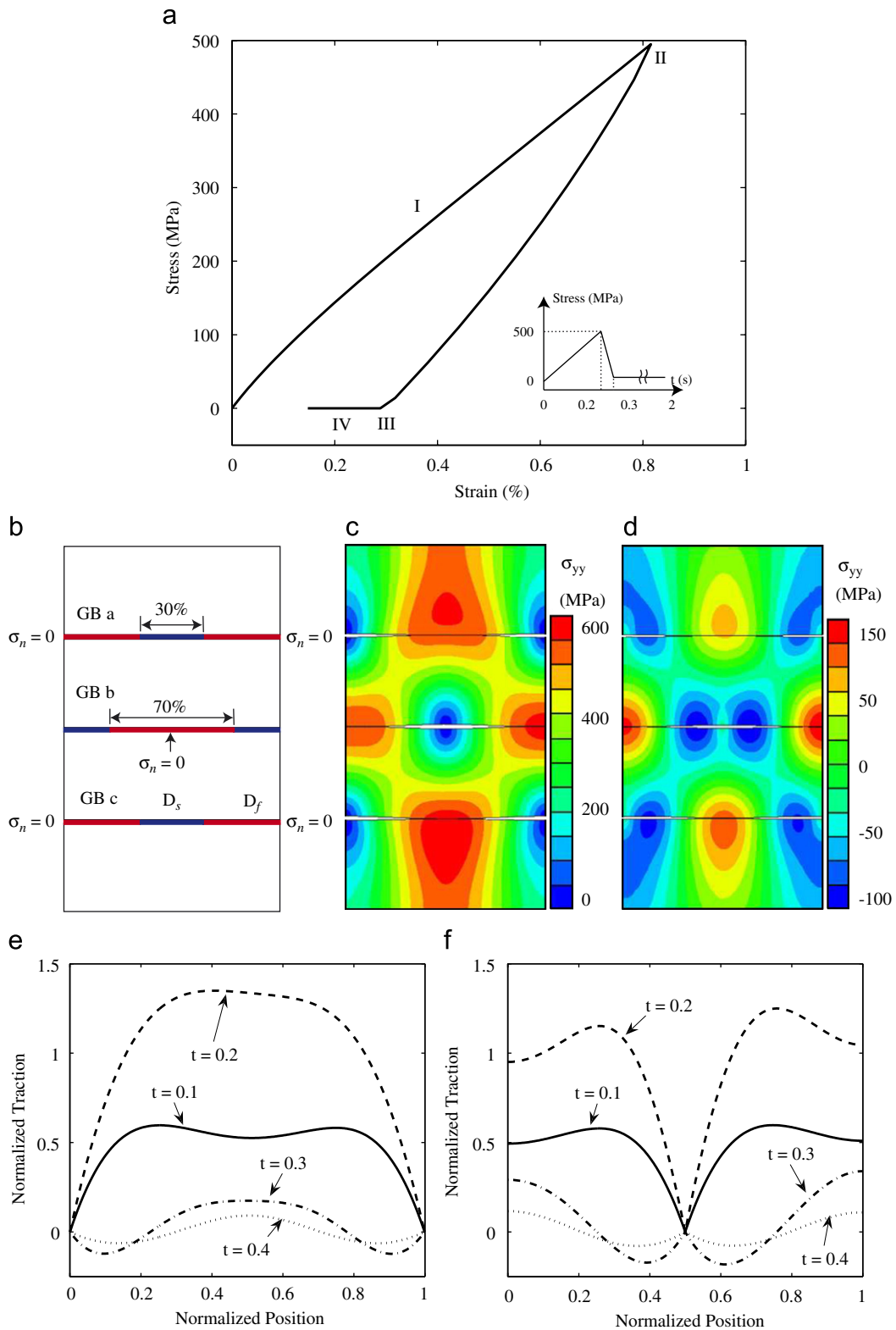


Fig. 15. Recoverable deformation in an idealized two-dimensional structure with heterogeneous GB diffusivity: (a) stress–strain curve for the structure shown in (b). The sample is subjected to a load–time profile shown in the inset; (b) a structure with three GBs, D_f and D_s represents fast and slow diffusion regions. Normal tractions nearby the two free surfaces in GB ‘a’ and GB ‘c’ and that at the middle point in GB ‘b’ is set to zero. Deformation and stress contour σ_{yy} : (c) at ‘II’ marked in (b); (d) that at ‘III’; (e) normal traction in GB a at different snapshot, the four time sequences correspond to ‘I’ to ‘IV’ marked in (b); (f) normal traction in GB ‘b’.

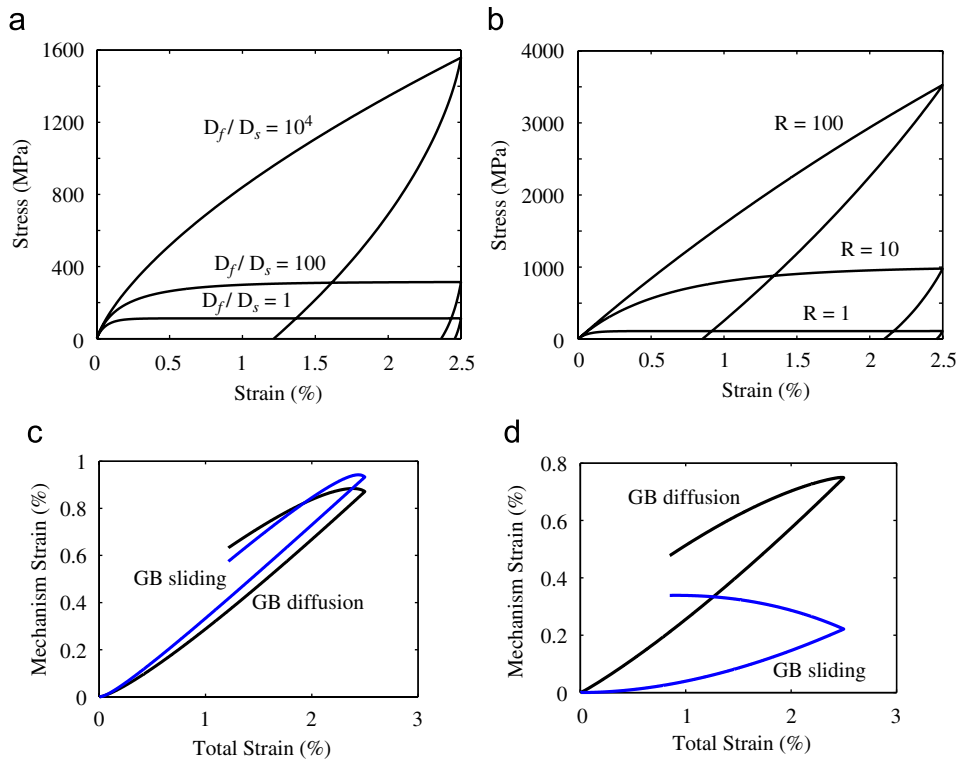


Fig. 16. Recoverable creep behavior due to heterogeneous GB diffusion and sliding using the microstructure in Fig. 6b: (a) stress–strain curves for several D_f/D_s ; (b) stress–strain curves for different R ; (c) evolution of mechanism strains during loading and unloading for the case of $D_f/D_s = 10^4$; (d) mechanism strain evolution for $R = 100$.

recoverable on unloading. A simple grain structure is chosen to show mechanical behavior by heterogeneous GB diffusion in individual GBs (Fig. 15b). The structure has three GBs, D_f and D_s represents fast and slow diffusion regions, respectively. Normal tractions nearby the two free surfaces in GB ‘a’ and GB ‘c’ and that at the middle point in GB ‘b’ are set to be zero. A stress boundary condition is applied to the top surface with a load–time profile shown in the inset in Fig. 15a. Corresponding stress–strain behavior is shown in Fig. 15a. Stress contours σ_{yy} at ‘II’ and ‘III’ marked in Fig. 15a are shown in Figs. 15c and d, respectively. The traction evolution with time in GB ‘a’ and GB ‘b’ are shown in Figs. 15e and f. During unloading, compressive stress develops in high diffusivity regions; the gradient of chemical potential in these GBs drives matter to diffuse out and recover a portion of plastic strain induced by GB diffusion.

Recovery of inelastic strain is further investigated using a more realistic microstructure shown in Fig. 6a. GBs marked with a square have a diffusivity of D_s and all others have a diffusivity of $D_f = D_0$. The sample is loaded at a constant strain rate of $10^{-5}/s$ to a nominal strain of 2.5% and then unloaded at $-10^{-5}/s$. We take the diffusivity–fluidity ratio $R = 1$ for each GB. Stress–strain curves at different ratios of D_f/D_s are shown in Fig. 16a. Mechanism strains contributed by GB diffusion and GB sliding (defined in Eq. (21)), in the case of $D_f/D_s = 10^4$, are shown in Fig. 16c. A significant fraction of inelastic strains contributed by both GB diffusion and GB sliding is recovered. Constrained GB sliding also can induce recoverable deformation. Here we assign the same diffusivity D_0 to all GBs and increase R by increasing GB viscosity η . Fig. 16b shows several stress–strain curves at different values of R . Mechanism strains contributed by GB diffusion and GB sliding are shown in Fig. 16d, for the case of $R = 100$. Inelastic strain by GB diffusion is found to be substantially recovered. Rajagopalan et al. (2007) have recently studied deformation in freestanding f.c.c. nanocrystalline thin films and reported that “plastic” deformation in these films is recoverable. The evidence that heterogeneous GB diffusion can induce recoverable “plastic” deformation may

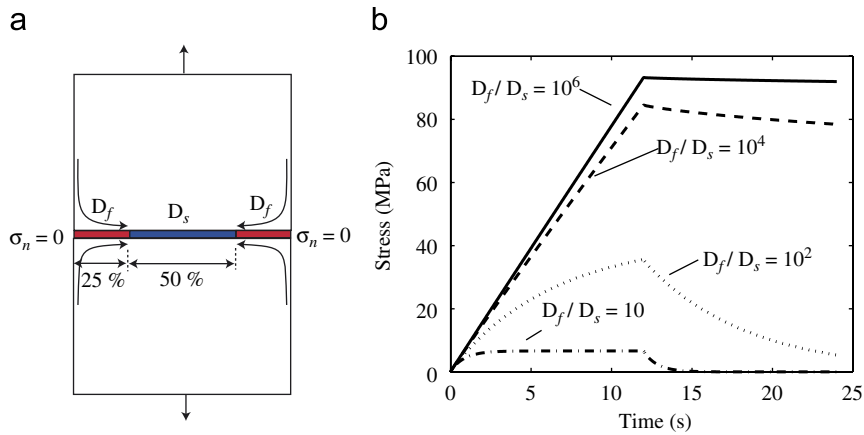


Fig. 17. Stress relaxation in a bi-diffusivity GB to show that stress relaxation is controlled by low diffusivity GBs. (a) The GB structure, GB diffusivity in the blue region is slower than those in the red regions. (b) Stress versus time for different values of D_f/D_s . Stress relaxation is controlled by the slow diffusion region.

suggest that diffusion has played an important role in the observed recovery of “plastic” deformation in their experiments.

3.5. Characteristic time for stress relaxation is controlled by low diffusivity GBs

The microstructure shown in Fig. 17a is also used to investigate the characteristic time for stress relaxation under heterogeneous GB diffusivity, with $D_f/D_0 = 10$. We apply displacement controlled boundary condition. The sample is loaded at a strain rate of $7.5 \times 10^{-4}/s$ in the first 12 s. The boundary is then fixed. Four simulation cases are conducted, with diffusivity in the middle half of the GB taken to be $D_s = D_0, D_0/10, D_0/100, D_0/10^5$. Fig. 17 shows that stress relaxation is much slower in the presence of heterogeneous GB diffusivity. For the case when $D_f/D_s = 10^6$, there is almost no stress relaxation in the time interval of 12 s. The low diffusivity parts of GBs are the primary load carrying regions and control the characteristic time scale for stress relaxation. Meanwhile, the deformation is mainly accommodated by the high diffusivity GBs.

4. A generalized Maxwell model for recoverable deformation

In order to develop simple intuitive understanding for recoverable inelastic deformation induced by heterogeneous GB diffusion and sliding, we consider a generalized Maxwell model shown in Fig. 18a, in which a high viscosity element η_h corresponds to a low diffusivity GB and a low viscosity element η_l corresponds to a high diffusivity GB. One could easily derive the stress–strain relationship for a given loading rates, either in strain or stress loading conditions.

We have taken the spring stiffness $K = 40$ GPa and dashpot viscosity $\eta_h = \eta_l = 10^7$ Pa s. The viscosity of 10^7 Pa s is obtained by matching the dimensionless equation for GB diffusion in Eq. (6) for polycrystalline Cu with $l = 100$ nm and at $T = 500$ K. A typical stress–strain curve for the structure under a constant strain rate of $1.5 \times 10^{-3}/s$ is shown in Fig. 18b, which resembles Fig. 3a obtained from polycrystalline aggregates with uniform GB diffusivity. Fig. 18c shows the overall stress–strain behavior as well as that in each element in the structure subjected to stress loading with $\eta_h = 5 \times 10^8$ Pa s and $\eta_l = 10^7$ Pa s. The sample is loaded at a stress-rate of 5 MPa/s and unloaded at -50 MPa/s. In the presence of heterogeneous viscosity, we see that the deformation is partially recoverable upon unloading. When the applied stress is fully removed, the element with low diffusivity is still in tension but that with high diffusivity is in compression. These internal stresses drive the structure to deform further while part of the strain is recovered, resembling the behavior shown in Fig. 15.

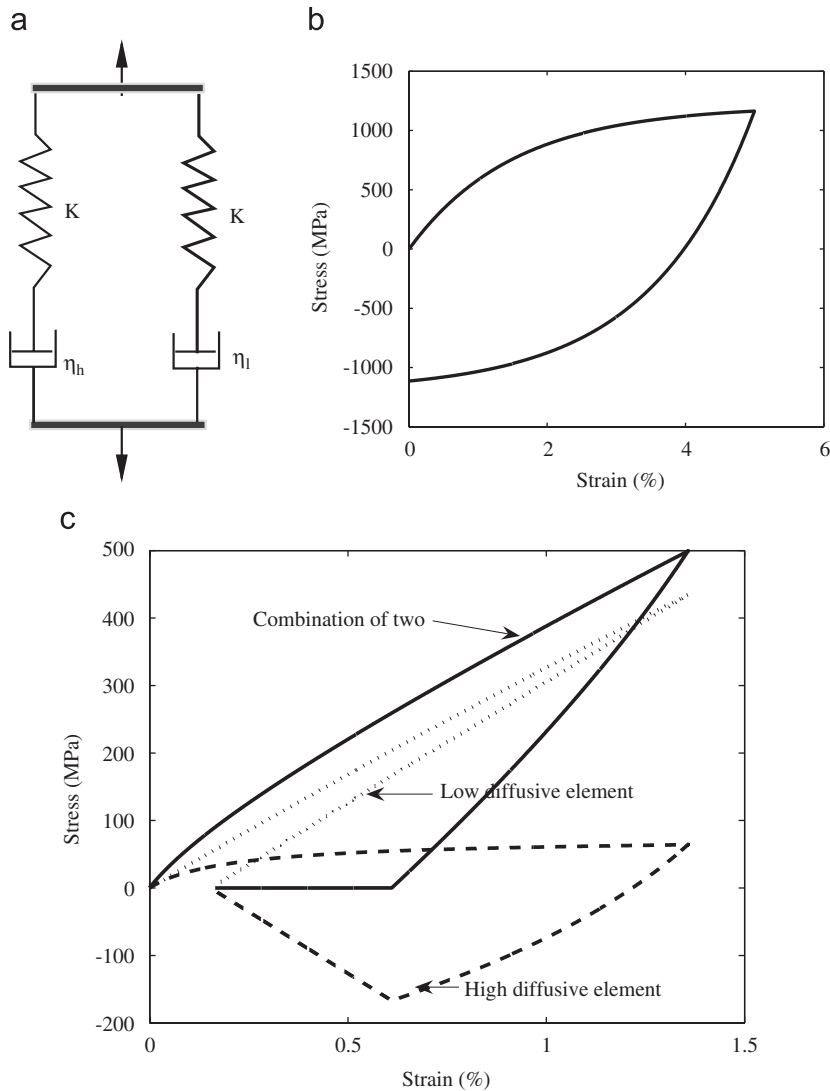


Fig. 18. A generalized Maxwell model is used to demonstrate that heterogeneous diffusion could give rise to recoverable creep deformation. (a) The model. (b) The stress–strain relation for $\eta_h = \eta_l$. (c) The overall stress–strain relation and that in the two elements for $\eta_h = 5 \times 10^8$ and $\eta_l = 10^7$ Pa.s. The high viscosity element has low diffusion.

5. Conclusion

We have carried out a preliminary investigation of diffusional creep in polycrystalline solids with heterogeneous GB diffusivities. The main observations from our analysis can be summarized as follows.

- Heterogeneous GB diffusion leads to time-dependent creep deformation which is partially recoverable over a characteristic time scale associated with diffusion on fast diffusion GBs. This recovery is driven by internal stresses induced by mismatches in GB diffusivity.
- Heterogeneous GB diffusion leads to severe stress concentration over the characteristic time scale associated with diffusion on high diffusivity GBs. However, over the long term, such stress concentration tends to attenuate as steady-state creep is approached.

- GB diffusion and sliding have to cooperate to allow compatible deformation field in polycrystals. A macroscopic creep rate is controlled by the slower processing of these two mechanisms. At steady state, each mechanism contributes half of the macroscopic creep rate.
- In polycrystals with bi-diffusivity, the deformation resembles that in a percolating system when GB diffusion is the rate-controlling mechanism. The transition from fast diffusion-controlled deformation to that by slow diffusion occurs in the region $0.4 < \phi < 0.7$ as ϕ decreases, here ϕ is the fraction of fast diffusion GBs. When deformation in slow diffusion GBs is completely constrained, an abrupt transition from GB accommodated creep to elastic deformation is seen at $\phi \approx 0.6$.
- Deformation is mainly accommodated by high diffusivity GBs while stress is primarily carried by low diffusivity GBs.
- On an intermediate time scale before steady-state creep is reached, high diffusivity GBs behave like cracks and result in severe stress concentration in low diffusivity GBs.
- The characteristic time scale controlling stress relaxation is determined by low diffusivity GBs.

Although GB diffusion is considered as the primary mechanism of mass transport in our analysis, dislocation emission–absorption in GBs can lead to additional mass transportation in conventional polycrystalline solids at high temperatures and for nanostructured materials even at room temperature. Such a scenario raises an interesting question of how GB diffusion is coupled to dislocation emission–absorption. GB migration can also influence mass transport and deformation in nanostructured materials, especially during thermal cycling. The coupling of various alternative and competing mechanisms including GB diffusion, GB migration, dislocation emission/absorption and GB sliding should play important roles in the deformation and reliability of small structures, e.g., metallic interconnects in electric circuits and nanocrystalline materials. Further studies of the coupling among different mechanisms are left to future work.

Acknowledgments

The research reported has been partially supported by the NSF MRSEC Program at Brown University under Award DMR-0520651. This support is gratefully acknowledged.

Appendix A

The analytical solutions for steady-state creep along a bi-diffusivity GB shown in Fig. 10 can be easily derived as follows. The diffusion equations in the two regions of the GB are

$$\frac{\partial u}{\partial t} = \dot{\epsilon} = \begin{cases} -D_f \frac{\partial^2 \sigma}{\partial x^2} & \text{for } x < 0, \\ -D_s \frac{\partial^2 \sigma}{\partial x^2} & \text{for } x > 0. \end{cases}$$

At steady state, the left side of the above equations is constant, and the general solutions can be written as

$$\sigma = \begin{cases} a_1(x+1)^2 + b_1(x+1) + c_1 & \text{for } x < 0, \\ a_2(x-1)^2 + b_2(x-1) + c_2 & \text{for } x > 0 \end{cases}$$

with boundary conditions:

$$\sigma = 0 \quad \text{at } x = -1, \tag{30a}$$

$$\sigma = 0 \quad \text{at } x = 1, \tag{30b}$$

$$j_{0+} = j_{0-} \quad \text{at } x = 0 \quad \text{flux continuity,} \tag{30c}$$

$$u_{0+} = u_{0-} \quad \text{at } x = 0 \quad \text{displacement continuity,} \tag{30d}$$

$$\mu_{0+} = \mu_{0-} \quad \text{at } x = 0 \quad \text{chemical potential continuity,} \quad (30e)$$

$$2\dot{\epsilon} = j_{x=-1} - j_{x=1} \quad \text{mass conservation,} \quad (30f)$$

$$\sigma_{\infty} = \frac{1}{2} \int_{-1}^1 \sigma \, dx \quad \text{force balance.} \quad (30g)$$

The normal traction profile along the GB can therefore be derived as

$$\sigma = \begin{cases} -\frac{\dot{\epsilon}}{2D_f}(x+1)^2 + \frac{\dot{\epsilon}(3D_f + D_s)}{2D_f(D_f + D_s)}(x+1) & \text{for } x < 0, \\ -\frac{\dot{\epsilon}}{2D_s}(x-1)^2 - \frac{\dot{\epsilon}(D_f + 3D_s)}{2D_s(D_f + D_s)}(x-1) & \text{for } x > 0 \end{cases} \quad (31)$$

and

$$\sigma_{\infty} = \frac{D_f^2 + 14D_fD_s + D_s^2}{24D_fD_s(D_f + D_s)} \dot{\epsilon}. \quad (32)$$

The maximum traction occurs at

$$x_m = \frac{D_f - D_s}{2(D_f + D_s)} \quad (33)$$

with value equal to

$$\sigma_{\max} = 3\sigma_{\infty} \frac{D_f(D_f + 3D_s)^2}{(D_f + D_s)(D_f^2 + 14D_fD_s + D_s^2)}. \quad (34)$$

The steady-state solution for the bi-diffusivity GB can be reduced to that of a GB with uniform diffusivity⁵ if $D_f = D_s = D_0$. At steady state, the stress concentration factor induced by heterogeneous GB diffusion for the sample Fig. 10 is $\sigma_{\max}/\sigma_{\infty} = 3$ if $D_f \gg D_s$.

References

- Abaqus Reference Manuals, 2005. Hibbit, Karlsson & Sorenson, Inc., Pawtucket, RI.
- Arzt, E., Ashby, M.F., Verrall, R.A., 1983. Interface controlled diffusional creep. *Acta Metall.* 31, 1977.
- Ashby, M.F., 1969. On interface-reaction control of Nabarro–Herring creep and sintering. *Scr. Metall.* 3, 837.
- Ashby, M.F., 1972. Boundary defects and atomistic aspects of boundary sliding and diffusional creep. *Surf. Sci.* 31, 498.
- Ashby, M.F., Verrall, R.A., 1973. Diffusion-accommodated flow and superplasticity. *Acta Metall.* 21, 149–163.
- Balk, T.J., Dehm, G., Arzt, E., 2003. Parallel glide: unexpected dislocation motion parallel to the substrate in ultrathin copper films. *Acta Mater.* 51, 4471–4485.
- Bower, A.F., Wininger, E., 2004. A two-dimensional finite element method for simulating the constitutive response and microstructure of polycrystals during high temperature plastic deformation. *J. Mech. Phys. Solids* 52, 1289–1317.
- Buehler, M.J., Hartmaier, A., Gao, H.J., 2003. Atomistic and continuum studies of crack-like diffusion wedges and associated dislocation mechanisms in thin films on substrates. *J. Mech. Phys. Solids* 51, 2105–2125.
- Cheng, S., Ma, E., Wang, Y.M., Keeskes, L.J., Youssef, K.M., Koch, C.C., Trociewitz, U.P., Han, K., 2005. Tensile properties of in situ consolidated nanocrystalline Cu. *Acta Mater.* 53, 1521–1533.
- Coble, R.L., 1963. A model for boundary diffusion controlled creep in polycrystalline materials. *J. Appl. Phys.* 34, 1679–1682.
- Cocks, A.C.F., 1992. Interface reaction controlled creep. *Mech. Mater.* 13, 165–174.
- Frost, H., Ashby, M.F., 1982. *Deformation-Mechanism Maps: The Plasticity and Creep of Metals and Ceramics*. Pergamon Press, Oxford.
- Gao, H.J., Zhang, L., Nix, W.D., Thompson, C.V., Arzt, E., 1999. Crack-like grain-boundary diffusion wedges in thin metal films. *Acta Mater.* 47, 2865–2878.
- Gleiter, H., 1989. Nanocrystalline materials. *Prog. Mater. Sci.* 33, 223–315.
- Guduru, P.R., Chason, E., Freund, L.B., 2003. Mechanics of compressive stress evolution during thin film growth. *J. Mech. Phys. Solids* 51, 2127–2148.

⁵For the same structure in Fig. 10 with uniform GB diffusivity, steady-state normal traction within the GB is $\sigma = -3\sigma_{\infty}(x^2 - 1)/2$ and $\dot{\epsilon} = 3\sigma_{\infty}D_0$.

- Hardy, G., Littlewood, J.E., Polya, G., 1934. *Inequalities*. Cambridge University Press, Cambridge.
- Hartmaier, A., Buehler, M.J., Gao, H.J., 2005. Multiscale modeling of deformation in polycrystalline thin metal films on substrate. *Adv. Eng. Mater.* 7, 1–5.
- Herring, C., 1950. Diffusional viscosity of a polycrystalline solid. *J. Appl. Phys.* 21, 437–445.
- Jiang, Z.H., Liu, X.L., Li, G.Y., Jang, Q., Lian, J.S., 2006. Strain rate sensitivity of a nanocrystalline Cu synthesized by electric brush plating. *Appl. Phys. Lett.* 88, 143115.
- Kobrinisky, M.J., Thompson, C.V., 1998. The thickness dependence of the flow stress of capped and uncapped polycrystalline Ag thin films. *Appl. Phys. Lett.* 73, 2429–2431.
- Nabarro, F.R.N., 1948. Report of a Conference on the Strength of Solids. Physical Society, London, p. 75.
- Needleman, A., Rice, J.R., 1980. Plastic creep flow effects in the diffusive cavitation of grain boundaries. *Acta Metall.* 28, 1315–1332.
- Pan, J., Cocks, A.C.F., 1993. Computer simulation of superplastic deformation. *Comput. Mater. Sci.* 1, 95–109.
- Rajagopalan, J., Han, J.H., Saif, M.T.A., 2007. Plastic deformation recovery in freestanding nanocrystalline aluminum and gold thin films. *Science* 315, 1831–1834.
- Sethian, J.A., Wilkening, J., 2003. A numerical model of stress driven grain boundary diffusion. *J. Comput. Phys.* 193, 275–305.
- Simmons, G., Wang, H., 1971. *Single Crystal Elastic Constants and Calculated Aggregate Properties*. The MIT Press, Cambridge, MA.
- Spingarn, J.R., Nix, W.D., 1978. Diffusional creep and diffusional accommodated grain rearrangement. *Acta Metall.* 26, 1389–1398.
- Thouless, M.D., Rodbell, K.P., Cabral Jr., C., 1996. Effect of a surface layer on the stress relaxation of thin films. *J. Vac. Sci. Technol. Vac. Surf. Films* 14, 2454–2461.
- Wei, Y.J., Anand, L., 2007. A constitutive model for powder-processed nanocrystalline metals. *Acta Mater.* 55, 921–931.
- Weiss, D., Gao, H., Arzt, E., 2001. Constrained diffusional creep in UHV-produced copper thin films. *Acta Mater.* 49, 2395–2403.
- Wilkening, J., Borucki, L., Sethian, J.A., 2004a. Analysis of stress-driven grain boundary diffusion. Part I. *SIAM J. Appl. Math.* 64, 1839–1863.
- Wilkening, J., Borucki, L., Sethian, J.A., 2004b. Analysis of stress-driven grain boundary diffusion. Part II: degeneracy. *SIAM J. Appl. Math.* 64, 1864–1886.
- Yamakov, V., Wolf, D., Phillpot, S.R., Gleiter, H., 2002. Grain-boundary diffusion creep in nanocrystalline palladium by molecular-dynamics simulations. *Acta Mater.* 50, 61–73.